# Achievement of continuous-wave 100 kW radiofrequency transmission by a 1.3 GHz high-power input coupler

Pragya Nama,[1,*] Dai Arakawa,[2] Eiji Kako,[2] Ashish Kumar,[1,2] Takako Miura,[1,2] Hiromitsu Nakajima,[2] Hiroshi Sakai,[1,2] and Kensei Umemori[1,2]

[1]*The Graduate University for Advanced Studies, SOKENDAI, Hayama, Kanagawa 2040115, Japan*
[2]*High Energy Accelerator Research Organization, KEK, Tsukuba, Ibaraki 3050801, Japan*

(Received 21 April 2026; accepted 25 September 2026; published 28 October 2026)

A high-power input coupler was developed at KEK to deliver 100 kW-class radiofrequency (rf) power in the continuous-wave (cw) mode at 1.3 GHz to a superconducting cavity. To mitigate thermal loads during high-power rf transmission, the coupler was engineered with active water cooling integrated into critical components, including a warm inner conductor, outer conductor, antenna, and rf window. The newly developed coupler underwent rf conditioning of up to 145 kW in the pulsed mode and 100 kW in the cw mode using a dedicated test stand at room temperature. The coupler successfully transmitted world-record cw 100 kW rf power at 1.3 GHz continuously for 10 h without any interlock event. During operation, the temperature rise of the warm inner conductor, the most thermally stressed component, was limited to 15 °C whereas the maximum observed temperature increase was 19 °C at the doorknob. Further power scaling was not constrained by the coupler itself. These results demonstrate that the newly developed coupler can reliably sustain cw rf transmissions exceeding 100 kW with excellent thermal performance.

DOI: 10.1103/2sn3-xls8

## I. INTRODUCTION

High-power radiofrequency (rf) input couplers capable of reliable continuous-wave (cw) operation at the 100 kW level are critical enabling technologies for next-generation superconducting radiofrequency (SRF) accelerators. This requirement is particularly stringent for compact high-intensity SRF accelerators, where the delivery of high cw rf power must be achieved while maintaining strict thermal stability, vacuum integrity, and long-term operational reliability.

Approximately 15 years ago, a fundamental high-power input coupler, known as the cERL injector coupler, was developed at KEK with the goal of transmitting an rf power of 100 kW in cw mode. Room-temperature high-power tests demonstrated rf transmissions of up to 200 kW in pulsed operation, 50 kW in cw operation, and short-duration operation at 100 kW in the cw mode [1]. However, severe overheating damaged the warm inner conductor during the extended high-power operation, which limited the stable cw power transmission to approximately 30–40 kW. These results highlight the dominant role of thermal constraints in limiting achievable cw rf power. Similar limitations have been reported previously. At Cornell University, a high-power injector coupler based on the TTF-III design achieved cw operation of up to 60 kW; however, further power scaling was restricted by the excessive temperature rise in the warm inner conductor [2]. The bERLinPro project developed a high-power coupler derived from the cERL injector design and demonstrated cw operation of up to 45 kW [3]. A low cryogenic load coupler has been developed at Fermilab [4]. Collectively, these efforts indicate that the thermal management of warm rf components, particularly the inner conductor and waveguide-to-coaxial transition, remains the principal challenge in achieving stable 100 kW-class cw operation.

Motivated by these challenges, KEK recently initiated the development of a 1.3 GHz, 100 kW-class high-power input coupler that is specifically optimized for cw operation and is compatible with conduction-cooled $Nb_3Sn$ SRF accelerators [5–7]. First, a detailed investigation of the design and high-power performance of the original cERL injector coupler was conducted to identify the dominant thermal and rf loss mechanisms. Based on the results of these studies, the design of the original cERL injector coupler was modified by incorporating active water cooling of the warm inner and outer conductors. High-power testing of this modified cERL injector coupler confirmed improved thermal performance and stable cw

*Contact author: pragya@post.kek.jp

*Published by the American Physical Society under the terms of the Creative Commons Attribution 4.0 International license. Further distribution of this work must maintain attribution to the author(s) and the published article's title, journal citation, and DOI.*

operation of up to 27 kW, validating the effectiveness of enhanced active cooling.

Finally, a new high-power input coupler was designed using comprehensive rf, thermal, and thermomechanical simulations. Active water cooling was integrated into all thermally stressed components of the new coupler, including the warm inner conductor, warm outer conductor, antenna, and rf window, to suppress the temperature rise under high-power cw operation. Detailed engineering designs were completed, and a prototype coupler was fabricated. Due to budgetary constraints, a single high-power coupler was manufactured and assembled into a room-temperature test stand by coupling it with a modified cERL injector coupler via a rectangular waveguide connection box.

rf conditioning and high-power testing were performed at the cERL facility at KEK in both the pulsed and cw modes. The newly developed coupler was successfully conditioned up to 145 kW in a pulsed operation and demonstrated a stable cw transmission of 100 kW for 10 h without any interlock event and with excellent thermal performance. Further power scaling is not limited by the coupler.

This paper presents the design, fabrication, and experimental validation results of a newly developed 100 kW-class cw high-power input coupler. The coupler design considerations are first described, followed by the fabrication, assembly, and experimental setup. The rf conditioning procedures and high-power test results in pulsed and cw modes are presented. Finally, the measured thermal behavior and multipacting characteristics were compared with the simulation results.

## II. COUPLER DESIGN

The design of the newly developed input coupler was based on a previously developed cERL injector coupler series. To date, three major design iterations of the cERL injector coupler have been realized.

The first version, referred to as the *prototype cERL injector coupler*, was the initial design, which was fabricated and tested at room temperature. High-power rf tests demonstrated a transmission of up to 200 kW in the pulsed mode, up to 50 kW in the cw mode, and a few minutes at 100 kW in the cw mode [1]. However, during these tests, severe overheating and damage to the warm inner conductor were observed, which ultimately limited the stable cw operation to approximately 30–40 kW.

Subsequently, a second version, referred to as the *original cERL injector coupler*, was developed to address these limitations and meet the integration requirements of the cERL injector cryomodules. In this design, the length of the warm inner conductor was increased to match the cryomodule geometry, and the impedance of the coaxial line was changed from 41.5 to 66 Ω in order to reduce the rf losses on the copper (Cu) surface [1]. The warm inner conductor was fabricated from oxygen-free Cu and equipped with water-cooling channels for active cooling during high-power operations. The water-cooling channels were brazed onto the warm outer conductor. This version demonstrates reliable performance and is currently installed in the cERL injector cryomodule, which has been routinely used for beam operation over the past 15 years [8].

In this study, the third version was developed by modifying only the warm section of the prototype cERL injector coupler. This configuration, referred to as the *modified cERL injector coupler*, incorporates water-cooling pockets in the warm inner conductor and a water-cooling jacket in the warm outer conductor to enhance the thermal management during high-power operation. The rf window and cold section were identical to those of the prototype coupler. High-power testing of this modified coupler demonstrated stable cw operation up to 27 kW limited by the capability of the high-power rf source (inductive output tube), confirming the effectiveness of active water cooling in suppressing the temperature increase, particularly in the warm inner conductor, which was the most thermally stressed component.

In this study, a new coupler design was introduced to achieve reliable cw rf transmission at the 100 kW level. To ensure stable rf transmission at 100 kW cw, a robust and efficient cooling strategy is essential. Significant thermal loads are expected owing to the rf-induced Ohmic losses, particularly along the inner conductor. Therefore, active water cooling was adopted instead of air cooling owing to its superior heat-transfer capability. To accommodate effective water cooling of the inner conductor, a coaxial-type coupler with a single rf window located at room temperature was selected. Although dual-window couplers provide additional protection for cavity vacuum, they significantly complicate the implementation of the cooling system.

The coupler was designed with fixed coupling to the cavity to reduce mechanical complexity and enable reliable water cooling. Adjustable coupling schemes typically require bellows in the inner conductor, which poses significant challenges for the implementation of active water cooling and introduces additional reliability concerns. A detailed sectional view of the newly designed coupler, along with the cooling scheme, is shown in Fig. 1. Further details of the rf, thermal, and mechanical designs are provided in Ref. [7].

The warm section of this input coupler consists of a warm outer conductor, a warm inner conductor, and a doorknob-type transition. The warm inner conductor was fabricated from oxygen-free Cu and incorporated into 0.2 mm thin Cu bellows to provide mechanical flexibility. A water-cooling pocket is brazed to the inner surface of the inner conductor immediately below the bellows. The upper and lower flanges of the inner conductor were composed of Cu-coated SUS304. The warm outer conductor was constructed from SUS304 with a 60–70 $\mu$m Cu coating on its

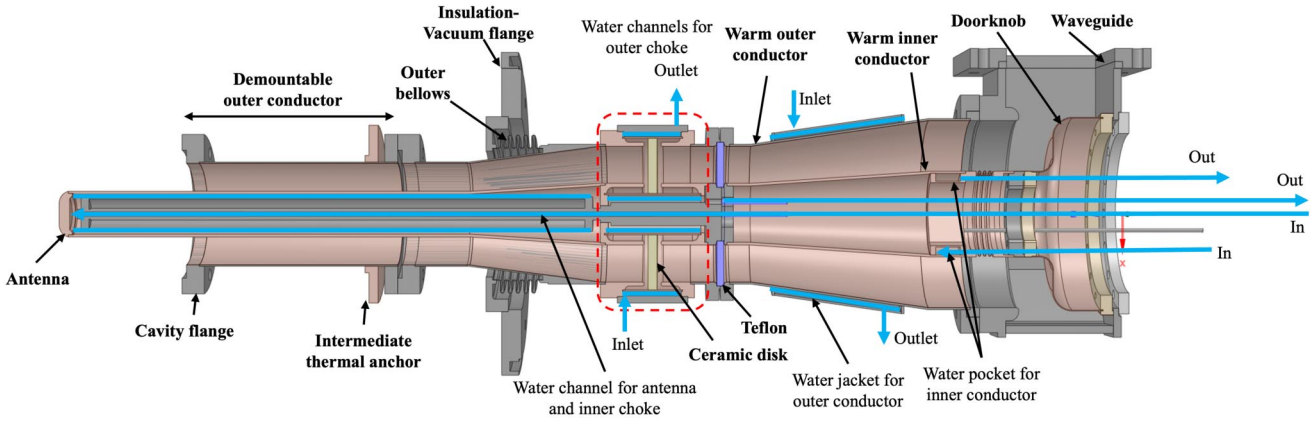



FIG. 1. Schematic cross section of a newly designed 1.3 GHz 100 kW class high-power coupler.

inner surface. An external water-cooling jacket was welded to the outer surface of the warm outer conductor to facilitate active cooling. The doorknob cup was fabricated from a 0.6-mm-thin Cu sheet for flexibility, whereas the upper and lower flanges of the doorknob were made of Cu-coated brass, and the waveguide was constructed from aluminum (Al 5052). The rf window of the coupler includes a disk-type ceramic (Alumina AO479U from Kyocera [9]) with a thickness of 6.8 mm, which is made up of high-purity (99.5%), low-loss alumina with a permittivity of 9.7 and loss tangent of $4 \times 10^{-5}$ [10]. To mitigate the impedance mismatch and minimize rf reflections, a choke structure based on the TRISTAN-type rf window design [11] was incorporated into the rf window assembly. Both the choke structure and antenna were fabricated from oxygen-free Cu and designed to accommodate active water cooling. To diagnose arc activity during high-power testing, an ICF 34 flange was installed on the vacuum side of the rf window.

The cold section of the coupler features a demountable outer conductor. The inner surface of the cold outer conductor was 10 μm Cu coated on 1 mm thick SUS304. The insulation-vacuum flange at the outer conductor incorporates bellows to provide flexibility against thermal shrinkage and expansion during thermal cycling. To cool the coupler effectively during rf transmission, the design incorporates water-cooling channels at the warm inner conductor, warm outer conductor, antenna, and rf window.

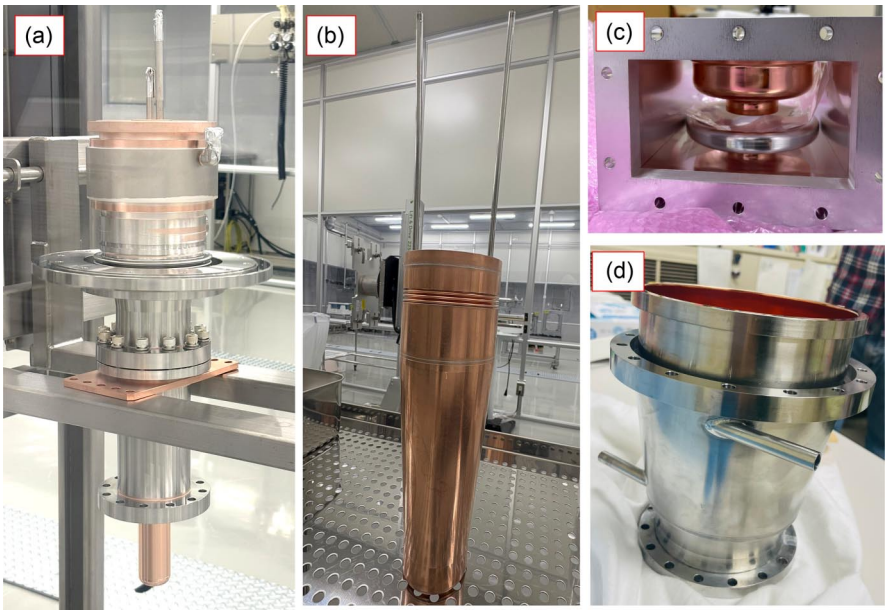



FIG. 2. (a) rf window with cold section, (b) warm inner conductor, (c) doorknob transition, and (d) warm outer conductor of the newly fabricated coupler.

## III. COUPLER FABRICATION AND ASSEMBLY

Following the finalization of the geometrical design and specifications, various companies commissioned the fabrication of the coupler components. The coupler was divided and fabricated into several parts, such as the rf window and cold section, along with a demountable outer conductor, warm inner conductor, warm outer conductor, doorknob transition waveguide, and Teflon plate. Figure 2 illustrates the rf window and cold section, warm inner conductor, doorknob transition, and warm outer conductor of the coupler. Figure 3 presents a flowchart of the steps carried out from coupler fabrication to the high-power test.

The rf window and the cold section of the coupler operate in a high-vacuum environment. Therefore, the thorough cleaning of these components is essential in clean environments. Cleaning was performed in class 1000 clean room at the COI (Superconducting Accelerator Promotion Center) facility at KEK. The components were rinsed with low-pressure ultrapure water and dried using an ionized air gun to remove remaining water. Subsequently, the components were placed in a Class 10 clean room for overnight drying. The coupler was subsequently encased in a plastic bag and transferred from the COI facility to the clean room at the cERL facility for assembly and construction of a test stand.

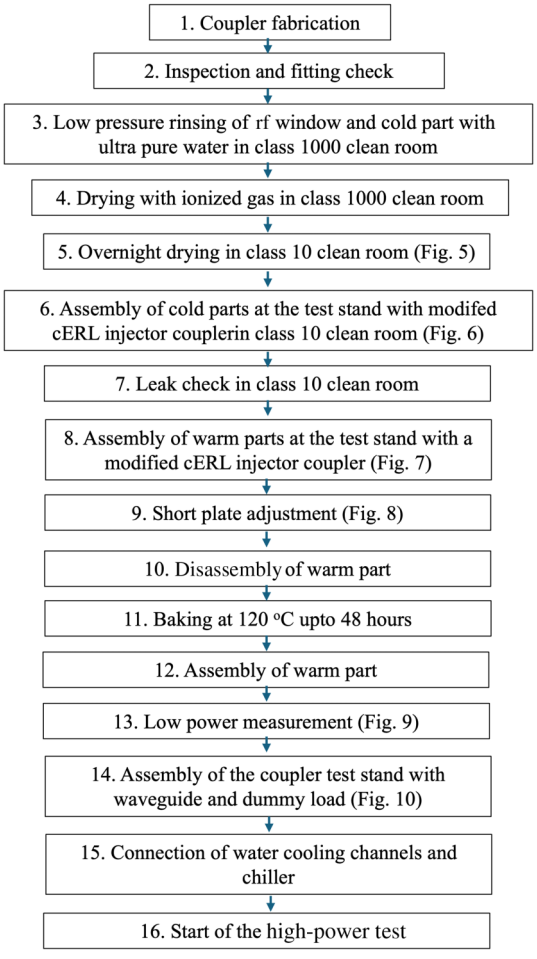



FIG. 3. Flowchart showing the steps followed from the coupler fabrication up to high-power test.

For the high-power test, the new coupler was assembled with the modified cERL injector coupler connected via a rectangular waveguide connection box. Helicoflex was used for vacuum sealing between the flanges. After tightening the cavity flange and the demountable outer conductor flange, a leak check was performed. Subsequently, the test stand was transferred outside the cERL clean room for the assembly of the warm-section components.

The warm-section components, including the inner conductor, outer conductor, and doorknob, were assembled for both couplers. For the new coupler, the short plate of the doorknob was initially left unwelded to facilitate precise adjustment at a target frequency of 1.3 GHz. To determine the optimal position, the short plate was progressively moved toward the doorknob cup, and low-power measurements of the $S$-parameter with respect to frequency were conducted using a network analyzer. Figure 4 shows the measured reflection coefficient ($S_{1,1}$) with respect to the position of the short plate of the doorknob at the test stand, along with the simulated $S_{1,1}$ for the new coupler. Based on these measurements, the optimal short plate position was identified, marked on the doorknob, and sent to the manufacturer for final welding.

To reduce outgassing and establish the clean, high-vacuum environment required for high-power rf conditioning, the rf window and cold section of the coupler were subjected to a baking process. This procedure is essential for minimizing the partial pressures of residual gases, particularly water vapor, which can degrade the vacuum

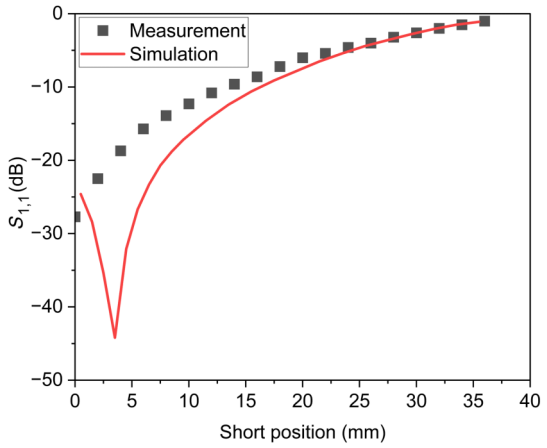



FIG. 4. Measured $S_{1,1}$ with respect to the short position of the doorknob at a frequency of 1.3 GHz for the coupler test stand and comparison with the simulated values of $S_{1,1}$ at 1.3 GHz for only one new coupler (here short position is defined as minimum distance between doorknob cup and short plate).

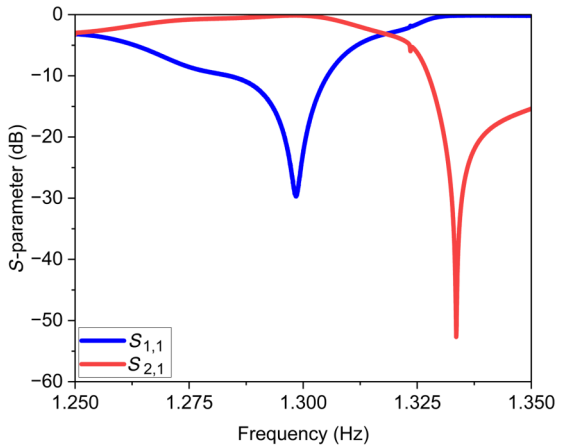



FIG. 5. Measured $S$-parameter with respect to the frequency for the coupler test stand ($S_{1,1}$ at 1.3 GHz = −22.5 dB and $S_{2,1}$ at 1.3 GHz = −0.02 dB).

quality. The baking was performed continuously at 100 to 120 °C for 48 h, during which a gradual decrease in pressure was observed, indicating effective outgassing. Following baking, the coupler test stand was slowly cooled to room temperature. A vacuum gauge was mounted on the rectangular waveguide connection box. Prior to baking, the vacuum level was $1.9 \times 10^{-5}$ Pa, while after baking, a final vacuum level of $1.6 \times 10^{-6}$ Pa was achieved, which was suitable for subsequent rf processing. After the coupler baking, the warm section of the coupler was assembled, and the $S$-parameter was measured. The measured $S_{1,1}$ at this stage was −22.5 dB at target frequency of 1.3 GHz, with a bandwidth of 4.6 MHz at −20 dB for the coupler test stand, satisfying the coupler design requirements, shown in Fig. 5. The fully assembled test stand was connected to the transmission line using flexible waveguide with water-cooling channels, as shown in Fig. 6.

## IV. EXPERIMENTAL SETUP

Figure 7 shows the experimental setup, in which a cw 300 kW klystron served as the rf power source. High-power rf was delivered from the klystron to the coupler test stand in both pulsed and cw modes. The forward and reflected power levels were measured using USB power sensors, and all the power meters and associated cables were calibrated prior to the high-power tests. The input power (Pf1) and reflected power (Pb1) were measured at the upstream coupler. Similarly, the transmitted power (Pf2) and reflected power (Pb2) were measured at the downstream coupler, as shown in Fig. 7. An interlock system was implemented to ensure safe operation and protect the experimental setup. A total of 17 temperature sensors were installed at various locations on the coupler test stand to monitor the temperature increase during the rf operation. Arc detectors were mounted at the viewports near the rf windows of both couplers, and cameras were installed at the viewport below the waveguide connection box to visually monitor activities inside the couplers. The coupler components, including the antenna, warm inner conductor, warm outer conductor, rf window, and waveguide bellows, were actively cooled using a water chiller. The temperature of cooled water at the chiller was controlled at temperature of 20 °C and for each component, flow rate of the water was 1 L/ min. In addition, forced-convection air cooling was applied using four small fans and one big fan during the high duty factor and cw rf operation.

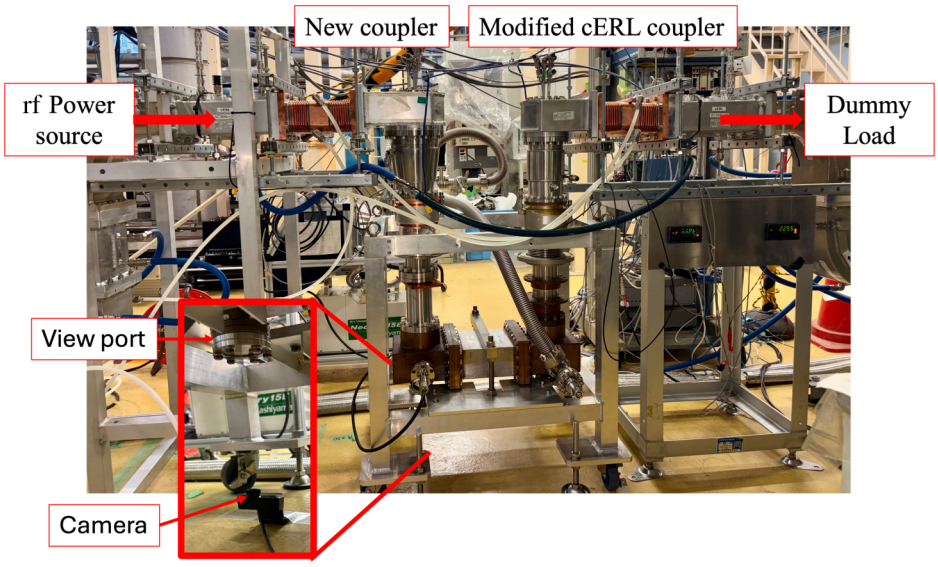



FIG. 6. Coupler test stand assembled with the waveguide for high-power test and location of the view port and camera to see the activities inside coupler.

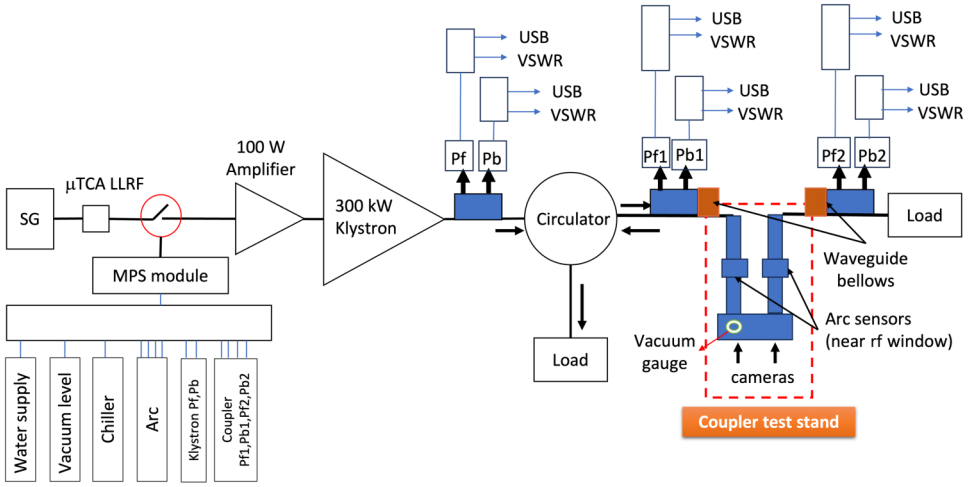



FIG. 7. Experimental setup for the high-power test of the coupler test stand [7].

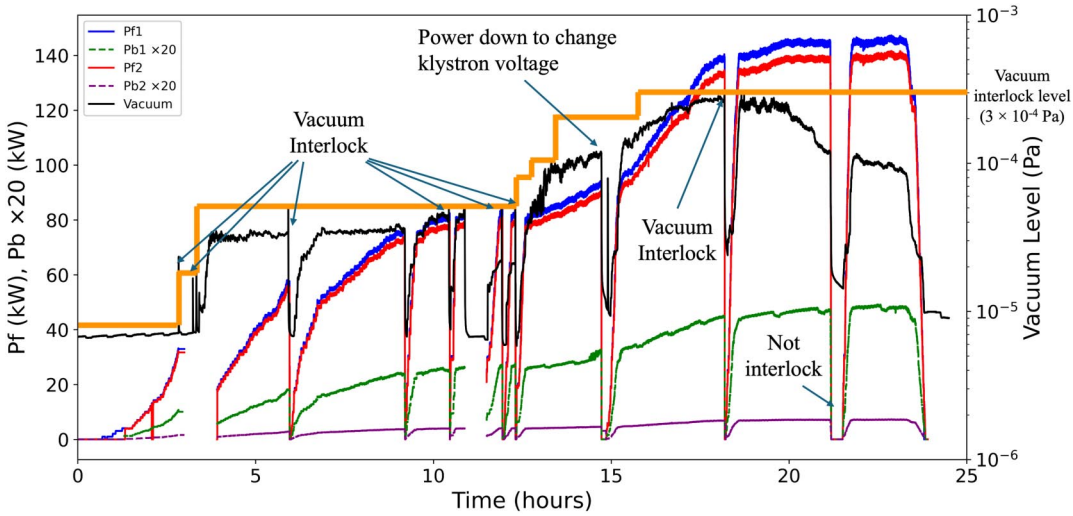



FIG. 8. Power level and vacuum pressure with time during rf conditioning in pulse mode with pulse width of 20 µs and pulse repetition rate of 5 Hz (here Pf1 and Pb1 are input and reflected power measured at upstream coupler, respectively, and Pf2 and Pb2 are transmitted and reflected power measured at downstream coupler, respectively).

## V. rf CONDITIONING

### A. Pulse mode

The rf conditioning was performed to avoid severe discharge events that could damage the couplers. rf conditioning of the coupler test stand was initially performed in the pulsed mode. The pulse repetition rate was fixed at 5 Hz, while the pulse width was increased stepwise from 20 µs to 60 ms. At each pulse width setting, the rf power was carefully ramped from 0 kW to a target level of 135–145 kW depending on the system stability. The vacuum interlock level was gradually increased as the rf power increases. Finally, vacuum interlock level was set at $3 \times 10^{-4}$ Pa. Once the maximum power was reached, it was maintained for 1–2 h to allow for effective surface conditioning and stabilization of the vacuum and temperature. The rf power was gradually reduced to 0 kW before the pulse width increased. Figure 8 illustrates the power level and vacuum pressure during rf conditioning in pulse mode with pulse width 20 µs. This process was repeated for successive pulse width settings, which were increased 5 times at each step, starting from 20 µs until a pulse width of 10 ms was reached. Figure 9 illustrates the power level and vacuum pressure during rf conditioning with pulse width 2.5 and 10 ms. Afterward, the pulse width was further extended to 20, 40, and 60 ms. The 60 ms pulse width corresponds to a duty factor of 30%. Figure 10 illustrates the power level and vacuum pressure during rf conditioning with pulse widths of 40 and 60 ms.

### B. cw mode

During pulsed rf conditioning at a pulse width of 60 ms and repetition rate of 5 Hz, corresponding to a duty factor

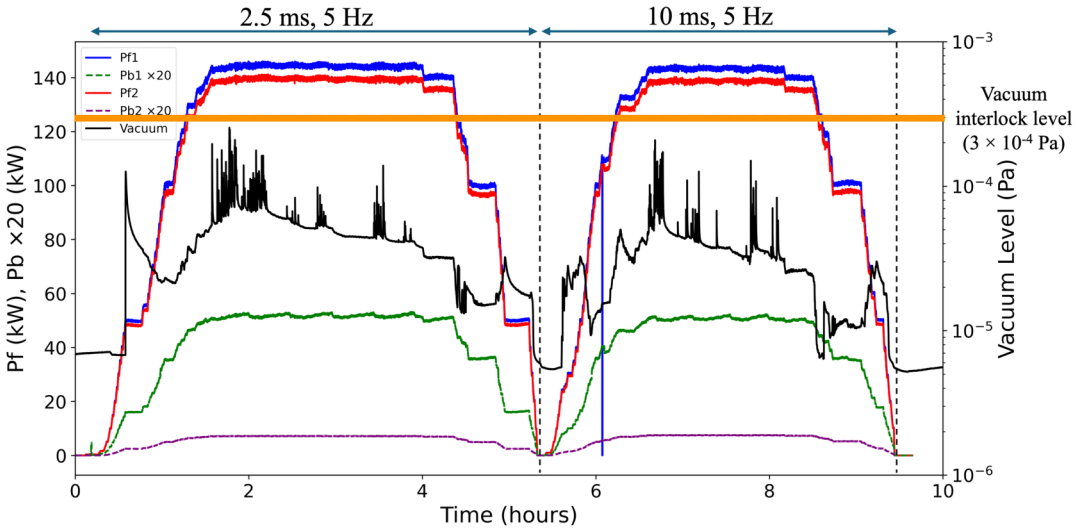



FIG. 9. Power level and vacuum pressure profile during rf conditioning with 2.5 ms pulse and 10 ms pulse width and pulse repetition rate of 5 Hz (here Pf1 and Pb1 are input and reflected power measured at upstream coupler, respectively, and Pf2 and Pb2 are transmitted and reflected power measured at downstream coupler, respectively).

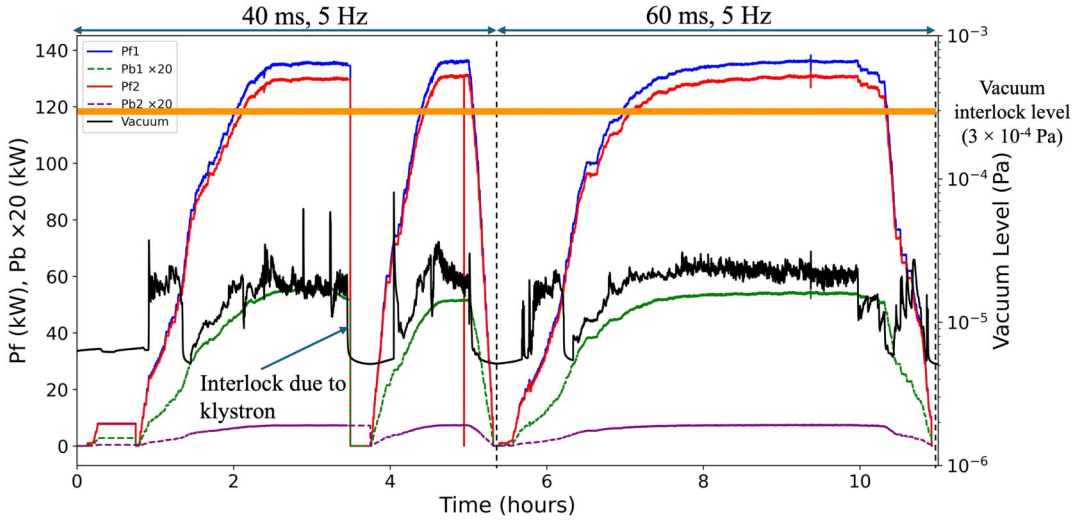



FIG. 10. Power level and vacuum pressure profile during rf conditioning with pulse width of 40 and 60 ms and pulse repetition rate of 5 Hz (here Pf1 and Pb1 are input and reflected power measured at upstream coupler, respectively, and Pf2 and Pb2 are transmitted and reflected power measured at downstream coupler, respectively).

of 30%, the coupler was operated at a maximum peak pulse power of 135 kW, resulting in an average power of approximately 40 kW. At this stage, the coupler test stand was considered sufficiently conditioned to transition to cw operation. For cw rf conditioning, the rf power was increased gradually from 0 to 100 kW in steps of 5 kW, with a ramp rate of 0.3–1 kW/ min, as shown in Fig. 11. The following day, a long-duration high-power test was conducted to evaluate the operational stability of the coupler test stand under sustained rf transmission at a cw power level of 100 kW. The rf power was gradually increased from 0 to 100 kW and maintained continuously for 10 h. No interlock events were triggered during the entire test period, indicating stable operation. Figure 11 shows the time evolution of the power level and vacuum pressure during cw operation. Hence, the coupler test stand consists of a new coupler and the modified cERL injector coupler successfully passed the final high-power transmission test, confirming its readiness for continuous operation at the design target power of cw 100 kW.

## VI. RESULTS OF HIGH-POWER TEST

### A. Conditioning time

The rf conditioning of the coupler test stand was conducted over a period of eight days, with a total

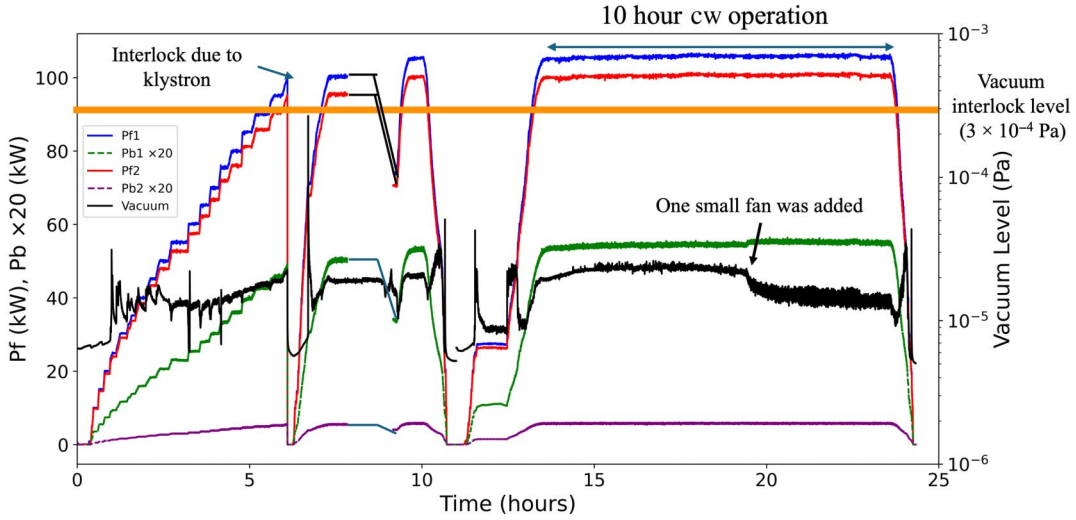



FIG. 11. Time evolution of the power level and vacuum pressure during cw operation up to 100 kW (here Pf1 and Pb1 are input and reflected power measured at upstream coupler, respectively, and Pf2 and Pb2 are transmitted and reflected power measured at downstream coupler, respectively).

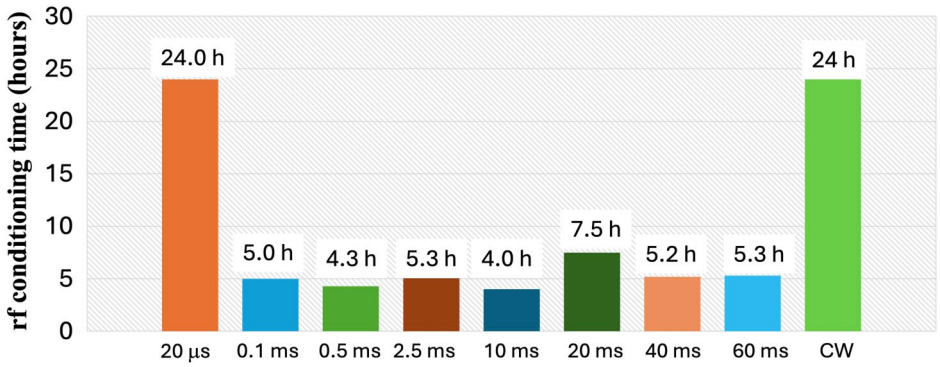



FIG. 12. rf conditioning time in pulse and cw mode.

accumulated conditioning time of approximately 84.6 h. Of this, 60.6 h were dedicated to pulse-mode conditioning, whereas the remaining 24 h were spent in cw mode. The initial conditioning stages employing short pulse widths (20 μs) required substantially longer durations because of the need for vacuum stabilization and frequent interlock events at lower power levels. In contrast, conditioning at longer pulse widths ($\geq$0.1 ms) progressed more rapidly, requiring shorter times to reach the target power levels. Figure 12 summarizes the rf conditioning times in both pulsed and cw modes.

### B. Vacuum versus power level

During rf conditioning in pulse-mode operation, a correlation was observed between the vacuum pressure and rf power level. Figure 13 illustrates the variation in vacuum pressure with respect to the rf power level during pulse conditioning. As the pulse width (i.e., duty factor) increased, the vacuum pressure exhibited a consistent improvement trend, particularly above 55 kW. This behavior indicates effective surface cleaning of the coupler components driven by rf processing. The gradual reduction in outgassing and stabilization of the vacuum at higher power levels and longer pulses suggest that the rf field helped desorb contaminants and adsorbed gases from the internal surfaces of the coupler. However, some vacuum activity consistently remained between the power levels of 20 and 55 kW, suggesting a possible multipacting region in this power range.

### C. Temperature profile

Figure 14 shows the locations of the 17 temperature sensors ($T_1 - T_{17}$) positioned on the coupler test stand. One temperature sensor ($T_{18}$) was intentionally left unattached to facilitate the measurement of the ambient temperature. Figure 15 presents the temperature evolution at these locations and the vacuum pressure during rf conditioning in cw mode. Figure 16 compares the

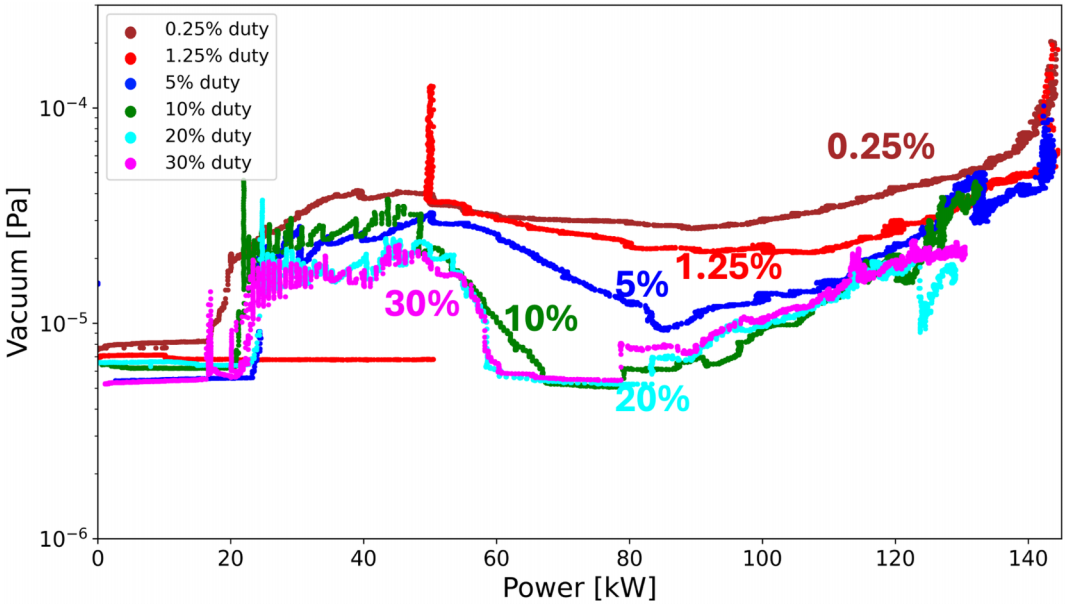



FIG. 13. Profile of vacuum pressure with respect to rf power level for different duty factors. (Here 0.25%, 1.25%, 5%, 10%, 20%, and 30% duty corresponds to for 0.5, 2.5, 10, 20, 40, and 60 ms pulse width, respectively.)

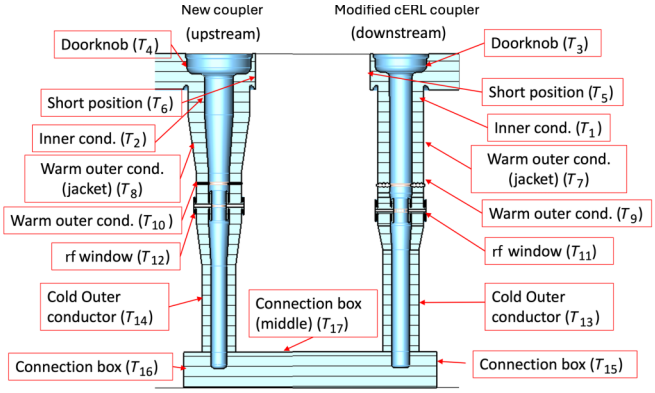



FIG. 14. Location of the temperature sensors on coupler test stand.

maximum temperature increases observed at different locations of the new coupler and the modified cERL injector coupler during long-duration cw operation at 100 kW. The ambient temperature during these measurements was between 23 and 25 °C.

For the newly developed coupler, the highest temperatures were observed at the doorknob ($T_4 = 43.0$ °C) and at the short position ($T_6 = 42.5$ °C). The temperatures of the warm inner and outer conductors were effectively suppressed by the active water cooling. In contrast, for the modified cERL injector coupler, the maximum temperature was observed at the doorknob ($T_3 = 78.6$ °C) and at the short position ($T_5 = 74.7$ °C). The new coupler significantly improved thermal performance due to its enlarged warm section, reducing rf power density

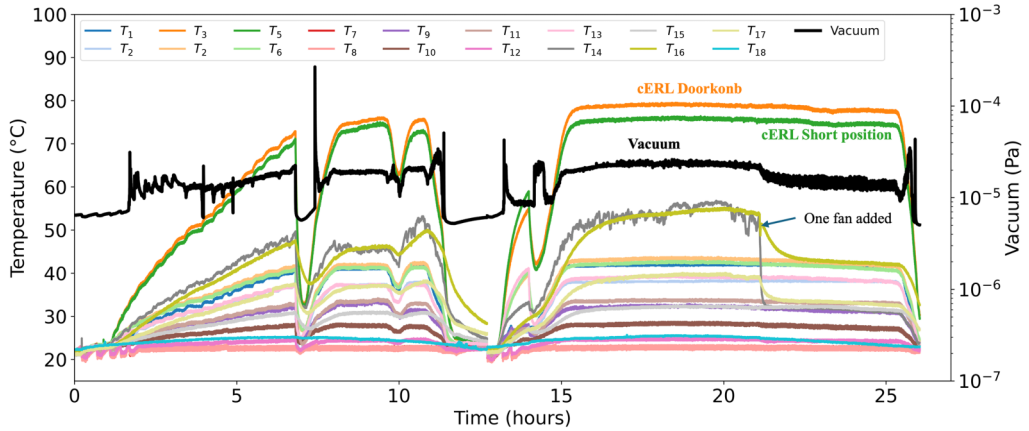



FIG. 15. Time evolution of temperature at various locations of temperature sensors and vacuum pressure during rf transmission in cw mode.

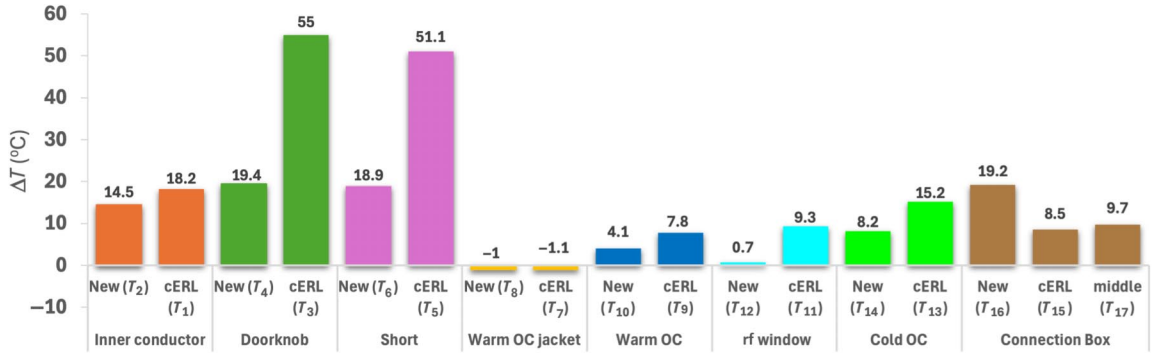



FIG. 16. Temperature rise along the different locations for the new coupler (New) and the modified cERL injector coupler (cERL).

compared to the modified cERL injector coupler. The surface area was increased by 24%, 15%, and 21% at the warm inner conductor, warm outer conductor, and doorknob, respectively. These results indicate that even a relatively small increase in coupler dimensions can lead to a significant reduction in temperature rise under high-power cw operation.

In previous high-power tests, the warm inner conductor of a cERL injector prototype coupler was identified as the most vulnerable component and was damaged by conditioning at a power level of cw 100 kW [1]. In contrast, during the present tests, the warm inner conductor temperatures remained well within safe limits, measuring $T_2 = 38.1\,°\mathrm{C}$ for the new coupler and $T_1 = 41.8\,°\mathrm{C}$ for the modified cERL injector coupler, demonstrating the effectiveness of the design of the warm inner conductor with water-cooling channels. The measured temperature profiles confirm that both couplers can withstand the substantial thermal loads generated during the cw rf transmission at 100 kW.

### D. Arc sensor signal

During the rf pulse conditioning, the arc-sensor signal was continuously monitored to detect potential discharges occurring near the rf window region of the couplers. Discharge phenomena can result from surface imperfections or residual gases and are typically associated with localized light emission. These emissions, even when faint, can be captured using an arc-sensor detection system. Light flashes may occur when the rf power processes the coupler surface. These lights are detected as spikes in the arc-sensor signal channel, allowing real-time assessment of the coupler surface activity. Figure 17(a) presents the arc- sensor signal (shown in pink) recorded during 0.5 ms pulse rf conditioning of the new coupler at a power level of 145 kW, along with the corresponding rf forward power (red), vacuum pressure (green), and interlock status (blue). As the rf conditioning progressed, the arc-sensor signal strength for the new coupler gradually weakened, indicating a reduction in activity as the surface became cleaner and more stable. Figure 17(b) presents the arc-sensor signal during 20 ms pulse processing at a power level of 100 kW, where no arc-sensor signal spikes were detected, confirming the successful conditioning effect.

The cERL coupler had previously (15 years ago) undergone rf conditioning up to a power level of 200 kW in pulse mode, resulting in a well-cleaned and stabilized rf surface [1]. Consequently, during the present rf conditioning, no activity was detected for this coupler.

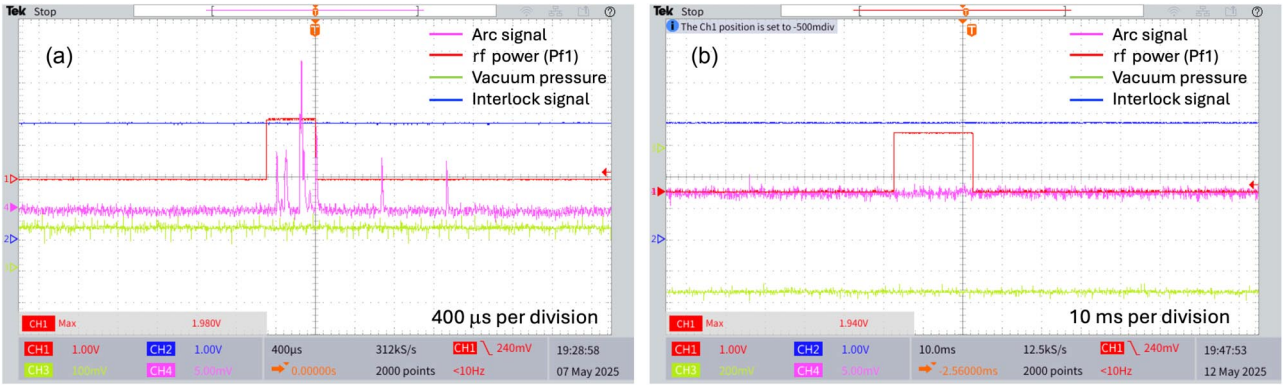



FIG. 17. Arc sensor signal in the new coupler during (a) 0.5 ms pulse processing at 145 kW, (b) 20 ms pulse processing at 100 kW. (Here, pink shows arc-sensor signal, red shows rf forward power, green shows vacuum pressure, and blue shows interlock signal.)

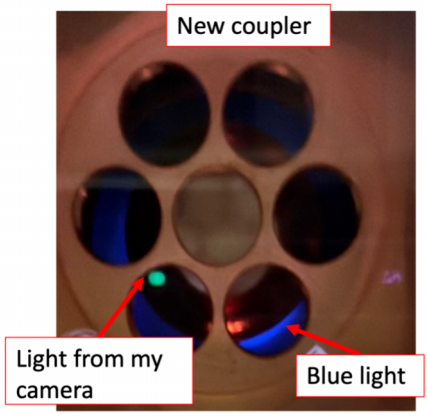



FIG. 18. Image from the new coupler's view port showing the observed blue light emission during rf conditioning at power level of 100 kW during cw operation. The photograph was captured using a mobile camera.

### E. Multipacting observation

During rf conditioning of the new coupler in pulsed mode with a pulse width of 0.5 ms, a flashing blue light was observed by the camera through the viewport. This light first appeared at the rf power levels of approximately 120 kW and persisted up to 145 kW for various pulse widths. In some instances, similar light emissions have been detected at power levels of approximately 50–55 kW. During cw conditioning, blue light was observed at 100 kW; however, its intensity was significantly weaker than that observed during pulsed operation. The occurrence of blue light is attributed to its multipacting activity. Figure 18 shows an image captured through the viewport of the new coupler during cw operation at an rf power of 100 kW when blue light was observed.

In contrast, no blue light is observed in the modified cERL injector coupler. This difference can be explained by the fact that the cERL injector coupler had already undergone extensive rf conditioning approximately 15 years earlier, reaching power levels of up to 200 kW in the pulsed mode [1], which likely suppressed multipacting through surface conditioning. The location of the camera is shown in Figs. 6 and 7.

## VII. INSIGHTS FROM THE SIMULATION STUDY

### A. Temperature profile

The detailed thermal simulations were performed to evaluate the steady-state temperature distribution of the coupler under high-power cw operation at room temperature. The applied thermal boundary conditions were set to 300 K for the components subjected to active water cooling, including the antenna, choke structure, warm

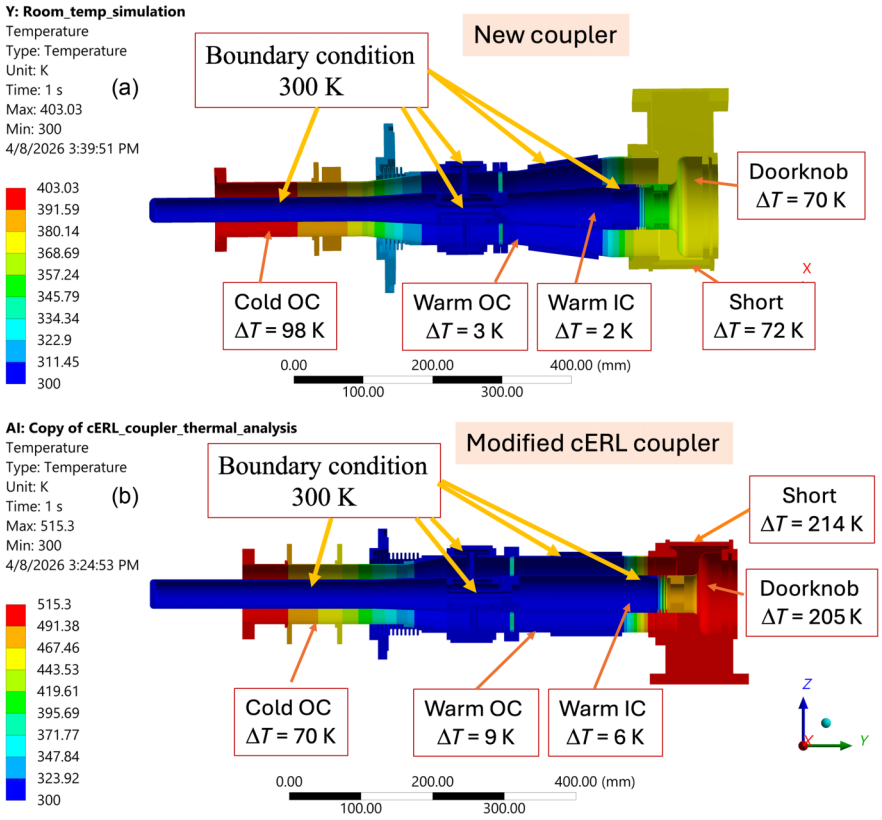



FIG. 19. Simulated temperature profile at 100 kW rf power transmission of the (a) new coupler and (b) modified cERL injector coupler, at room temperature condition (no convection boundary condition was considered during simulation).

TABLE I. Comparison of simulated and experimental temperature rise (at the doorknob) of the new coupler and modified cERL injector coupler.

| | Simulated $\Delta T$ at doorknob | Experimental $\Delta T$ at doorknob |
|---|---|---|
| New coupler | 70 K | 19.4 K |
| Modified cERL injector coupler | 205 K | 55 K |
| % reduction in temperature | 66% | 65% |

inner conductor, and warm outer conductor. Additionally, heat flux boundary conditions were applied for 100 kW rf power on the rf surfaces with electrical conductivity at room temperature. Figure 19 shows the simulated temperature profile of the new coupler and modified cERL injector coupler under cw 100 kW rf power and Table I compares the simulated and experimental temperature rise at the doorknob for both couplers. In the experiments, additional fan cooling was applied at the doorknob, leading to lower measured temperatures. Despite the difference in cooling conditions (no convection in simulation vs forced air cooling in experiment), the relative reduction in temperature rise is consistent. Under identical boundary conditions, the new coupler exhibited a temperature rise at the doorknob about 2–3 times lower than that of the modified cERL injector coupler. In contrast, the temperature rise at the cold outer conductor (OC) was higher in the new coupler due to its increased power density compared to the modified cERL injector coupler. The cold OC diameter of the new coupler is 78 mm, whereas the modified cERL injector coupler has a diameter of 82 mm. The significant reduction in temperature of the new coupler is attributed to the enlarged warm section. The surface area was increased by 24%, 15%, and 21% for the warm inner conductor, warm outer conductor, and doorknob, respectively, resulting in a reduction in rf power loss per unit area by 31%, 27%, and 50% at the corresponding locations. The exact quantitative relationship between local rf power loss density and temperature rise is complex, but the trend clearly indicates that reducing power density leads to improved thermal performance. Overall, both simulation and experimental results confirm that a modest increase in the size of the warm section significantly reduces temperature rise, thereby improving the thermal performance of the coupler. The performance of the coupler under cryogenic operating conditions was discussed in detail in Ref. [7].

### B. Multipacting

In the early stages of rf conditioning in the pulsed mode, the vacuum pressure consistently deteriorated over a wide power range from 20 to 145 kW, as shown in Fig. 20 (for 0.25% duty). During cw conditioning, the overall vacuum pressure showed improvement; however, the residual vacuum activity remained in the power ranges of 20–55 kW, above 80 kW, and up to 100 kW. This vacuum behavior suggests the possible presence of at least two distinct multipacting bands within these power ranges. The multipacting simulation at different regions of the coupler was performed using CST studio [7]. Figure 20 compares the measured vacuum pressure for the early conditioning stage (pulse) and final conditioning stage (cw) with the simulated growth rate of the number of particles for 100 °C, 200 °C, and a clean Cu surface with respect to the power level. A positive growth rate of the particles

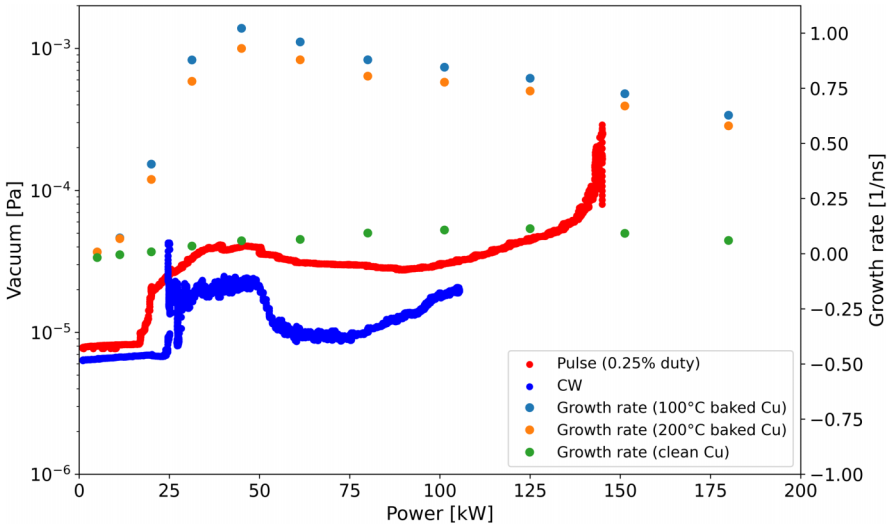



FIG. 20. Vacuum pressure with respect to rf power level during rf conditioning in pulse mode with pulse width 100 μs and cw mode (left $y$ axis), and simulated growth rate of total number of particles with respect to power level for 100 °C baked Cu, 200 °C baked Cu, and clean Cu surface (right $y$ axis).

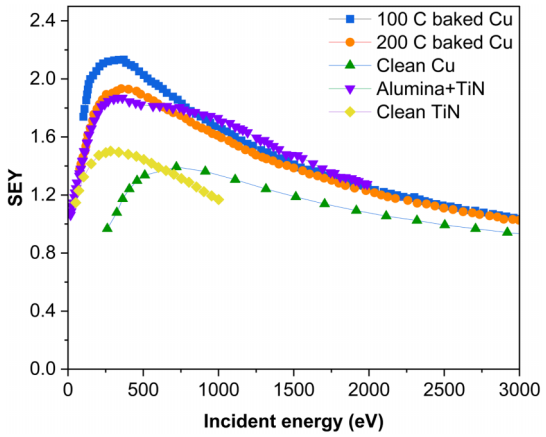



FIG. 21. SEY with respect to the incident energy of 100 °C baked [12], 200 °C baked [12], and clean Cu surface after rf conditioning [13] and alumina with TiN coating [14], and clean TiN after rf conditioning [13].

indicates the presence of multipacting electrons. For 100 and 200 °C baked Cu surfaces, the multipacting growth rate gradually increases and reaches a maximum around 45 kW. Afterward, it decreases. The growth rate for 200 °C baked Cu is slightly lower than for 100 °C baked Cu due to a lower SEY (see Fig. 21). For the clean Cu surface, the simulated growth rate is nearly zero, indicating that changes in surface conditions due to baking or rf conditioning affect the behavior of multipacting electrons. As rf conditioning progressed, the SEY of Cu surfaces and TiN coatings decreased. Figure 21 shows SEY for Cu at 100 °C, 200 °C, and after rf conditioning. It also shows SEY for alumina with TiN coating and clean TiN after rf conditioning. Due to the continuously evolving rf surface conditions, it is challenging to identify the precise locations of the multipacting zones with certainty. Nevertheless, the results demonstrate that, with systematic rf conditioning up to the required power levels, stable operation of the coupler can be achieved.

## VIII. DISCUSSION

High-power testing of the newly developed coupler showed stable rf power transmission of up to 100 kW in cw mode and 145 kW in pulsed mode. The power limit was primarily due to the power-handling capability of the circulator, not the coupler itself. To foresee the capability of this new coupler design, following aspects needs to be considered.

Thermal limitation: During long-duration cw operation up to 100 kW, the maximum temperature was 43 °C at the doorknob and 38 °C in the inner conductor. Implementing water-cooling channels at the doorknob would improve power transfer. Experimental results and thermal extrapolations suggest the coupler has a significant performance margin beyond 100 kW cw operation. Further optimization of auxiliary components and cooling design could enable cw rf transmission at several hundred kilowatts.

Multipacting limitation: Multipacting can be a limiting factor for achieving cw rf transmission above 100 kW. In this study, multipacting was identified by blue light emission in the new coupler, whereas no such behavior was observed in the modified cERL injector coupler. The following are the differences in the new coupler design and modified cERL injector coupler design which could affect the multipacting behavior: (i) *Geometry:* Both couplers have geometrically identical rf windows, although the modified cERL injector coupler uses alumina with $\epsilon = 9.2$, $\tan\delta = 4 \times 10^{-4}$, while the new coupler uses alumina with $\epsilon = 9.7$, $\tan\delta = 4 \times 10^{-5}$, (ii) *Coating parameters:* Both ceramic windows were coated with a 10 nm TiN layer (as per specification) on the vacuum side. However, controlling the coating thickness is challenging, and even a slight variation in coating thickness could alter the surface condition. The cold outer conductor configurations also differ as the modified cERL injector coupler has a 20–30 μm Cu coating, whereas the new coupler has a demountable design with a thinner 10 μm Cu layer, (iii) *Cleaning and baking:* Both couplers underwent similar cleaning and baking procedures, however, the modified cERL injector coupler was baked 3 times in its lifetime, compared to only once for the new coupler, (iv) *rf conditioning:* The modified cERL injector coupler was previously (15 years ago) conditioned up to 200 kW in pulsed mode, while the new coupler was conditioned up to 145 kW.

rf conditioning is known to reduce surface contaminants and lower the secondary electron yield (SEY), thereby suppressing multipacting. In this work, conditioning up to 145 kW enabled stable cw operation at 100 kW in the new coupler, although occasional light emission was still observed without any sustained discharges. Further conditioning is expected to reduce SEY and mitigate multipacting; however, at power levels above cw 100 kW, predicting its behavior becomes difficult. Whether conditioning alone is sufficient to eliminate multipacting at higher cw power remains uncertain and requires further study. The observed blue light and vacuum pressure fluctuations suggest a correlation with multipacting, although their exact relationship is not yet fully understood. Overall, comparison with the previously conditioned modified cERL injector coupler indicates that sufficient high-power rf conditioning, particularly in short-pulse mode, can significantly reduce or eliminate multipacting.

## IX. CONCLUSION

This paper presents the development and experimental validation of a 1.3 GHz 100 kW-class cw high-power input

coupler designed for SRF cavities. A new coupler design was presented to cater to the 100 kW rf transmission in cw mode. This new coupler was fabricated by various companies and assembled with the modified cERL injector coupler to construct a high-power test stand.

High-power rf conditioning was carried out in the pulsed mode up to 145 kW, followed by cw operation up to 100 kW. During rf operation, active water cooling was applied to the thermally stressed components, including the antenna, rf window, and warm section, while additional forced air cooling was employed to further dissipate the rf-generated heat. The newly developed coupler successfully transmitted 100 kW of rf power in the cw mode continuously for 10 h without any failure or interlock event. Notably, the maximum achievable power during testing was limited by the rf circulator rather than by the coupler itself, indicating a substantial performance margin for high-power operation. Excellent thermal performance was demonstrated, with a temperature rise of only 14.5 °C at the warm inner conductor which was the most thermally stressed component, and a maximum temperature increase of 19 °C observed at the doorknob.

In conclusion, this study demonstrates the successful development of a high-power input coupler capable of sustained 100 kW cw rf transmission at 1.3 GHz, representing the highest cw power level reported to date for a coupler test stand at this frequency.

## ACKNOWLEDGMENTS

Special thanks are given to T. Hara (KEK), T. Okada (K-vac), and H. Yamada (NAT) for experimental preparation. This research was supported by the JST and the establishment of university fellowships for the creation of science and technology innovation (Grant No. JPMJFS2136) and partially supported by the U.S.-Japan Science and Technology Cooperation Program in High Energy Physics and a JSPS Grant-in-Aid for Scientific Research (KAKENHI) Grant No. JP24K03208.

## DATA AVAILABILITY

The data that support the findings of this article are not publicly available upon publication because it is not technically feasible and/or the cost of preparing, depositing, and hosting the data would be prohibitive within the terms of this research project. The data are available from the authors upon reasonable request.

[1] E. Kako, S. Noguchi, T. Shishido, K. Watanabe, and Y. Yamamoto, High power test of CW input couplers for cERL injector cryomodule, in *Proceedings of the 3rd International Particle Accelerator Conference, New Orleans, LA, 2012* (IEEE, Piscataway, NJ, 2012), p. 2230, https://proceedings.jacow.org/IPAC2012/papers/weppc012.pdf.

[2] V. Veshcherevich, S. Belomestnykh, M. Liepe, V. Medjidzade, H. Padamsee, V. Shemelin, N. Sobenin, and A. Zavadtsev, Design of high power input coupler for Cornell ERL injector cavities, in *Proceedings of the 12th International Workshop on RF Superconductivity, Cornell University, Ithaca, NY* (JACoW, Geneva, Switzerland, 2005), p. 590, https://proceedings.jacow.org/SRF2005/papers/ThP54.pdf.

[3] A. Neumann, RF conditioning of 120 kW CW 1.3 GHz high power couplers for the bERLinPro energy recovery Linac, in *Proceedings of the 20th International Conference on RF Superconductivity, SRF2021, East Lansing, MI* (JACoW. Geneva, Switzerland, 2021), p. 216, https://proceedings.jacow.org/srf2021/papers/moptev007.pdf.

[4] S. Kazakov, Superconducting cavity coupler, U.S. Patent No. US10, 448, 496 (2019), https://www.osti.gov/biblio/1600183.

[5] P. Nama, A. Kumar, D. Arakawa, K. Umemori, E. Kako, H. Sakai, and T. Miura, Experimental result of high-power transmission through 1.3 GHz cERL injector prototype coupler, in *Proceedings of the 20th Annual Meeting of Particle Accelerator Society of Japan, PASJ2023, Funabashi, Chiba, Japan* (2023), p. 1105, https://www.pasj.jp/web_publish/pasj2023/proceedings/PDF/THP5/THP57.pdf.

[6] P. Nama, A. Kumar, D. Arakawa, K. Umemori, E. Kako, H. Sakai, and T. Miura, Effective thermal load mitigation in cERL injector coupler through warm section modification, in *Proceedings of LINAC'24*, Chicago, IL, USA (2024), p. 778, https://proceedings.jacow.org/linac2024/pdf/THPB073.pdf.

[7] P. Nama, D. Arakawa, E. Kako, A. Kumar, T. Miura, H. Nakajima, H. Sakai, and K. Umemori, Development of continuous-wave 100 kW-class high power input coupler for conduction-cooled L-band $Nb_3Sn$ accelerators, Nucl. Instrum. Methods Phys. Res., Sect. A **1083**, 171155 (2025).

[8] H. Sakai *et al.*, Stable operation of a fully energy-recovered 1-mA-class electron beam at a compact energy-recovery linac, Phys. Rev. Accel. Beams **28**, 091603 (2025).

[9] Kyocera Global, Low dielectric loss tangent, high strength, and high purity alumina, https://global.kyocera.com/prdct/fc/technologies/013.html.

[10] Y. Yamamoto, H. Yoshizumi, K. Nakamura, Y. Yamamoto, and S. Michizono, Research on ceramic for RF window, in *Proceedings of the 20th International Conference on RF Superconductivity, SRF2021, East Lansing, MI* (JACoW, Geneva, Switzerland, 2021), p. 771, https://proceedings.jacow.org/srf2021/papers/thpfdv008.pdf.

[11] S. Noguchi, E. Kako, and K. Kubo, Couplers—Experience at KEK, in *Proceedings of the 4th Workshop on RF Superconductivity, KEK, Tsukuba, Japan* (JACoW, Geneva, Switzerland, 1989), p. 397, https://proceedings.jacow.org/SRF89/papers/srf89e04.pdf.

[12] I. Bojko, N. Hilleret, and C. Scheuerlein, Influence of air exposures and thermal treatments on the secondary

electron yield of copper, J. Vac. Sci. Technol. A **18**, 972 (2000).

[13] W. Xu *et al.*, Broadband high power rf window design for the BNLElectron Ion Collider, Phys. Rev. Accel. Beams **25**, 061001 (2022).

[14] D. Wang, Z. Mao, Z. Ye, Y. Cai, Y. Li, Y. He, K. Qi, Y. Xu, and Q. Jia, Ultralow electron emission yield achieved on alumina ceramic surfaces and ist application in multipactor suppression, J. Phys. D **55**, 455301 (2022).